Immunity
Article

Roquin Paralogs 1 and 2 Redundantly Repress the Icos and Ox40 Costimulator mRNAs and Control Follicular Helper T Cell Differentiation

Katharina U. Vogel,[1,13] Stephanie L. Edelmann,[1,13] Katharina M. Jeltsch,[1] Arianna Bertossi,[2] Klaus Heger,[2] Gitta A. Heinz,[1] Jessica Zöller,[3] Sebastian C. Warth,[1] Kai P. Hoefig,[1] Claudia Lohs,[1] Frauke Neff,[4] Elisabeth Kremmer,[1] Joel Schick,[5] Dirk Repsilber,[7] Arie Geerlof,[6] Helmut Blum,[8] Wolfgang Wurst,[5,9,10,11] Mathias Heikenwälder,[3] Marc Schmidt-Supprian,[2,*] and Vigo Heissmeyer[1,12,*]

[1]Institute of Molecular Immunology, Helmholtz Zentrum München, Marchioninistrasse 25, 81377 Munich, Germany
[2]Max Planck Institute of Biochemistry, Am Klopferspitz 18, 82152 Martinsried, Germany
[3]Institute for Virology, Technische Universität München/Helmholtz Zentrum München, 81675 Munich, Germany
[4]Institute of Pathology
[5]Institute of Developmental Genetics
[6]Institute of Structural Biology
Helmholtz Zentrum München, Ingolstädter Landstrasse 1, 85764 Neuherberg, Germany
[7]Leibniz Institute for Farm Animal Biology, Dummerstorf, Wilhelm-Stahl Allee 2, 18196 Dummerstorf, Germany
[8]Laboratory for Functional Genome Analysis, Gene Center, Ludwig-Maximilians-Universität München, Feodor Lynen Strasse 25, 81377 Munich, Germany
[9]Max-Planck-Institute of Psychiatry, Kraepelinstrasse 2-10, 80804 Munich, Germany
[10]Technische Universität München, Lehrstuhl für Entwicklungsgenetik c/o Helmholtz Zentrum München, Ingolstädter Landstrasse 1, 85764 Neuherberg, Germany
[11]Deutsches Zentrum für Neurodegenerative Erkrankungen e. V. (DZNE), Site Munich, Schillerstrasse 44, 80336 Munich, Germany
[12]Ludwig-Maximilians-Universität München, Institute for Immunology, Goethestrasse 31, 80336 Munich, Germany
[13]These authors contributed equally to this work
*Correspondence: supprian@biochem.mpg.de (M.S.-S.), vigo.heissmeyer@helmholtz-muenchen.de (V.H.)
http://dx.doi.org/10.1016/j.immuni.2012.12.004

SUMMARY

The Roquin-1 protein binds to messenger RNAs (mRNAs) and regulates gene expression posttranscriptionally. A single point mutation in Roquin-1, but not gene ablation, increases follicular helper T (Tfh) cell numbers and causes lupus-like autoimmune disease in mice. In T cells, we did not identify a unique role for the much lower expressed paralog Roquin-2. However, combined ablation of both genes induced accumulation of T cells with an effector and follicular helper phenotype. We showed that Roquin-1 and Roquin-2 proteins redundantly repressed the mRNA of inducible costimulator (Icos) and identified the Ox40 costimulatory receptor as another shared mRNA target. Combined acute deletion increased Ox40 signaling, as well as Irf4 expression, and imposed Tfh differentiation on CD4$^+$ T cells. These data imply that both proteins maintain tolerance by preventing inappropriate T cell activation and Tfh cell differentiation, and that Roquin-2 compensates in the absence of Roquin-1, but not in the presence of its mutated form.

INTRODUCTION

T cells are required for humoral immune responses in which they give help to B cells in the germinal center. This function is provided by specialized CD4$^+$ follicular helper T cells (Tfh cells) that express the chemokine receptor CXCR5, the costimulatory molecules PD-1 and Icos, the transcription factor Bcl6 as well as the cytokine interleukin-21 (IL-21) (Crotty, 2011). Only recently, Tfh cells have been established among Th1, Th2, Th17, and Treg cell subsets by demonstrating that Bcl6 is the subset-determining transcription factor (Johnston et al., 2009; Nurieva et al., 2009; Yu et al., 2009). Tfh cell differentiation has been proposed to occur in a step-wise manner (Crotty, 2011). Priming by dendritic cells triggers upregulation of Icos on T cells, which is required for the expression of Bcl6. Bcl6 in turn induces CXCR5 expression (Choi et al., 2011), which allows T cell migration toward the T and B cell boundaries of follicles in the secondary lymphoid organs (Ansel et al., 1999; Kim et al., 2001). There, the contact to B cells and sufficient costimulation through several receptor-ligand pairs is required for the maintenance of Tfh cells (Crotty, 2011). The initial upregulation and sustained expression of Bcl6 (Baumjohann et al., 2011) is crucial for Tfh cell differentiation, but additional transcription factors like c-Maf and Batf (Bauquet et al., 2009; Betz et al., 2010; Ise et al., 2011; Kroenke et al., 2012) cooperate in the program. Furthermore, mice deficient for Irf4 cannot develop follicular helper T cells (Bollig et al., 2012; Kwon et al., 2009), and Irf4 cooperates with Stat3 to regulate gene expression downstream of IL-21 stimulation (Kwon et al., 2009). In contrast, Blimp1, which is induced through IL-2 and Stat5 signaling, counteracts commitment to this subset (Johnston et al., 2009, 2012; Nurieva et al., 2012). The transcription factors involved in Tfh cell differentiation also play a role in other subsets, suggesting functional plasticity. In fact, it was recently shown that during Th1 cell

differentiation, the cells pass through a stage shared with Tfh cells, which is marked by simultaneous expression of IL-21, interferon-γ (IFN-γ), Bcl6, and T-bet. Subsequent input from cytokines like IL-12 and balanced regulation of epigenetics and gene expression then either enforces Th1 or Tfh cell commitment (Nakayamada et al., 2011). Plasticity of the differentiation program has also been demonstrated in an IL-21 reporter mouse model in vivo (Lüthje et al., 2012). Because autoreactive Tfh cell numbers are important players in the development of autoimmune disease (Hu et al., 2009; Linterman et al., 2009b), the cellular transition point to the Tfh cell subset has to be tightly controlled. The molecular basis for this decision is yet to be defined.

Posttranscriptional gene regulation is well established in the control of several cellular transition points in immune cells (Hoefig and Heissmeyer, 2008). Roquin-1 (Rc3h1) is an RNA-binding protein that posttranscriptionally downregulates Icos messenger RNA (mRNA) expression (Athanasopoulos et al., 2010; Glasmacher et al., 2010; Yu et al., 2007). It recognizes the 3′untranslated region (3′UTR) of Icos mRNA and interacts with the enhancer of decapping Edc4 and the helicase Rck that promote mRNA decay (Glasmacher et al., 2010). A single point mutation in Roquin-1 (named Roquin-1^{san}) leads to a lupus-like autoimmune phenotype in mice, marked by enhanced numbers of Tfh cells and spontaneous germinal center formation (Vinuesa et al., 2005). These findings imply an important role for Roquin-1 in Tfh cell differentiation or homeostasis. San/san mice develop anti-nuclear and anti-DNA antibodies and show elevated surface expression of Icos on all T cells (Vinuesa et al., 2005). This suggests that increased Icos costimulation could lead to the autoimmunity observed in the san/san mouse. In fact, a number of studies show that experimentally induced constitutive costimulation, which is normally restricted in a spatial or temporal manner, can trigger autoimmunity. One example is the activation-induced tumor necrosis receptor superfamily 4 (*Tnfrs4* or *Ox40*) on T cells. Mice with ectopic coexpression of the Ox40 ligand on T cells develop autoimmune and autoinflammatory phenotypes and have anti-DNA antibodies in the serum (Murata et al., 2002). In line with this notion, CD28-deficiency, which normally prevents germinal center reactions, is functionally reconstituted in the context of the san/san genotype (Linterman et al., 2009a). Conversely, heterozygosity of Icos partially rescues san/san-associated phenotypes (Yu et al., 2007). However, increased Icos surface expression on all T cells is also observed in mice that lack Roquin-1 in T cells or in the hematopoietic system, but fail to elicit elevated follicular helper T cell numbers or anti-nuclear antibody responses (Bertossi et al., 2011). These findings question the previous concept in which impaired posttranscriptional gene regulation of Icos mRNA by the Roquin-1^{san} protein leads to increased differentiation or expansion of autoreactive Tfh cells, which then cause autoimmunity.

We have investigated the function of the paralog of Roquin-1, *Rc3h2* (Roquin-2) or also named Mnab, which has been previously described as a nucleic acid binding protein (Siess et al., 2000). Both proteins share a similar organization of the really interesting new gene (RING) finger, ROQ domain, and zinc finger (Athanasopoulos et al., 2010). Here, we demonstrate that Roquin-2 and Roquin-1 have redundant functions in T cells. Both proteins posttranscriptionally repressed Icos and Ox40 mRNA targets. T cells deficient in both Roquin-1 and Roquin-2 acquired a Tfh cell phenotype in the absence of immunization implying that Roquin-2 sufficiently controls Tfh cell differentiation upon Roquin-1 ablation. In contrast, in the *sanroque* mouse strain Roquin-2 cannot complement, suggesting that the Roquin-1^{san} protein is able to inhibit Roquin-2 function.

RESULTS

Rc3h2 Gene Deficiency Causes Postnatal Death

To determine the redundant and nonredundant roles of the Roquin-1 and Roquin-2 paralogs (*Rc3h1* and *Rc3h2*), we analyzed mice with a conditional *Rc3h2* allele and generated a monoclonal antibody that detected both proteins with similar efficiencies (Figure 1A; see Figures S1A–S1E available online; data not shown; EUCOMM mouse IKMC Project ID: 30078). We demonstrated complete absence of both proteins when we analyzed double genetically ablated *Rc3h1*$^{-/-}$; *Rc3h2*$^{-/-}$ (*Rc3h1-2*$^{-/-}$) mouse embryonic fibroblast (MEF) cells by immunoblotting. In wild-type (WT) mouse tissues, we found that Roquin-1 and -2 protein amounts were highest in extracts from lymph node and thymus and slightly lesser amounts were detected in extracts from brain, lung, and spleen (Figure 1B). Both proteins were only weakly detectable in extracts from heart, muscle, and kidney. Interestingly, in all tissues analyzed, Roquin-1 protein amounts were increased over Roquin-2 (Figure 1B). Likewise, protein extracts from CD4$^+$ T cells contained five times more Roquin-1 than Roquin-2 protein (Figure S1F).

The insertion of the neomycin resistance gene cassette abolished Roquin-2 expression (Figure 1A), rendering *Rc3h2*^{neo} a null allele. We found that *Rc3h2*$^{neo/neo}$ mice were born at Mendelian ratio (Figure 1C), but very few individuals reached adulthood (Figures 1C and 1D). A large proportion of *Rc3h2*$^{neo/neo}$ mice died within the first days after birth, and the strain exhibited decreased viability until weaning age (P20) (Figure 1D). The previously observed malformation of the tail and impairment of neural tube closure in *Rc3h1*-deficient mice was not observed in newborn *Rc3h2*-deficient mice (data not shown). However, similar to *Rc3h1*-deficient mice that die shortly after birth (Bertossi et al., 2011), newborn *Rc3h2*$^{neo/neo}$ mice revealed a somewhat immature lung phenotype with decreased expansion of alveoli and delayed clearance of amnion fluid from the alveolar space (Figure S1G). Although the exact cause of death remains unknown, it was overcome by crossing the mice on an outbred genetic background of Naval Marine Research Institute (NMRI) mice (Figure S1H). A similar strategy conferred a partial rescue of lethality in *Rc3h1*-deficient mice (Bertossi et al., 2011). The few surviving male and female *Rc3h2*$^{neo/neo}$ individuals on the C57BL/6 background appeared healthy and were fertile (data not shown). They had a phenotype of smaller size and decreased body mass compared with WT littermates (data not shown), which, on the outbred NMRI genetic background, was only seen in male individuals (Figure 1E).

Deletion of *Rc3h2* Does Not Affect Immune Cell Homeostasis

To analyze Roquin-2 function specifically in T cells, we generated *Rc3h2*$^{fl/fl}$; *Cd4-cre* mice. Roquin-2 protein was hardly

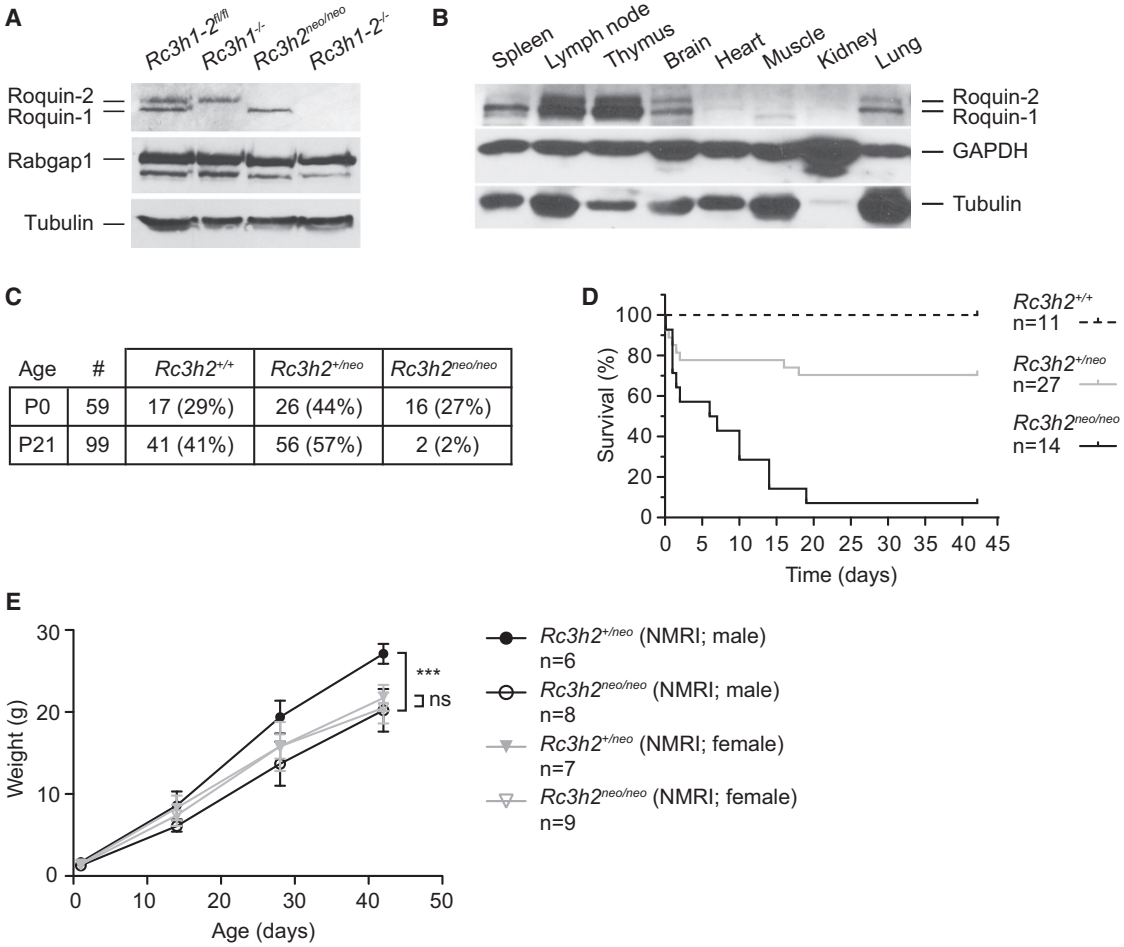

Figure 1. Systemic Deletion of *Rc3h2* Results in Postnatal Lethality and Reduced Body Size

(A) Immunoblot analysis of Roquin-1, Roquin-2, Rabgap1 (the *Rabgap1* gene is located 5′ adjacent to *Rc3h2*), and tubulin expression in *Rc3h1-2*$^{fl/fl}$, *Rc3h1*$^{-/-}$, *Rc3h2*$^{neo/neo}$ (Roquin-2-deficient), and *Rc3h1-2*$^{-/-}$ immortalized MEFs. *Rc3h1-2*$^{-/-}$ cells were obtained by retroviral cre transduction of *Rc3h1-2*$^{fl/fl}$ MEFs.

(B) Protein expression of Roquin-1 and Roquin-2 in different tissues with tubulin and GAPDH as loading controls. Data are representative for two (A, Rabgap1), three (A, Roquin-1, Roquin-2), and four (B) experiments.

(C) Genotype frequency of offspring from intercrosses of *Rc3h2*$^{+/neo}$ mice.

(D) Kaplan-Meier survival curves of mice with the indicated genotypes.

(E) Body-weight curves of male or female mice on a Naval Marine Research Institute (NMRI) outbred strain genetic background. Weight reduction in male *Rc3h2*$^{neo/neo}$ mice was already significant at day 1. Genotypes are indicated in the figure, and statistical significances were calculated by Student's t test (***$p < 0.001$). Data are represented as mean ± SD. See also Figure S1.

detectable in extracts from mature CD4$^+$ T cells (Figure 2A, left panel), and strongly reduced in thymocyte extracts (Figure 2A, right panel) of these mice. Compared to controls, *Rc3h2*$^{fl/fl}$*; Cd4-cre* mice showed no difference in thymocyte development (Figure 2B) and no differences in T cell CD62L and CD44 surface marker expression that discriminate naive from effector or memory T cells (Figure 2C). Furthermore, *Rc3h2*$^{fl/fl}$*; Cd4-cre* mice did not show increased Icos surface expression on single positive thymocytes or peripheral T cells (Figure 2D). Similar to *Rc3h1*$^{fl/fl}$*; Cd4-cre* mice (Bertossi et al., 2011), *Rc3h2*$^{fl/fl}$*; Cd4-cre* mice showed no differences in the percentage of follicular helper T cells (Tfh) or germinal center (GC) B cells (Figure 2E; Figure 2F). Even in *Rc3h2*-deficient animals, the immune cell homeostasis appeared normal, when we analyzed *Rc3h2*$^{neo/neo}$ mice on a mixed C57BL/6 and NMRI background (Table S1). Our analyses therefore did not reveal a nonredundant role for Roquin-2 in peripheral T cells or other immune cells.

Roquin-1 and Roquin-2 Redundantly Control T Cell Homeostasis

The normal immune system in *Rc3h2*-deficient mice (Figure 2; Table S1) and the comparatively mild immune dysregulation seen in *Rc3h1*-deficient mice (Bertossi et al., 2011) contrast the excessive autoimmunity that is observed in *Rc3h1*$^{san/san}$ mice (Vinuesa et al., 2005). This prompted us to investigate a functional redundancy of both genes in the T cell-specific combined gene ablation in *Rc3h1-2*$^{fl/fl}$*; Cd4-cre* mice (Figure 3A). Already at young age, these animals developed lymphadenopathy and splenomegaly with increased spleen weight and cellularity (Figure 3B). The mice exhibited a decreased frequency of

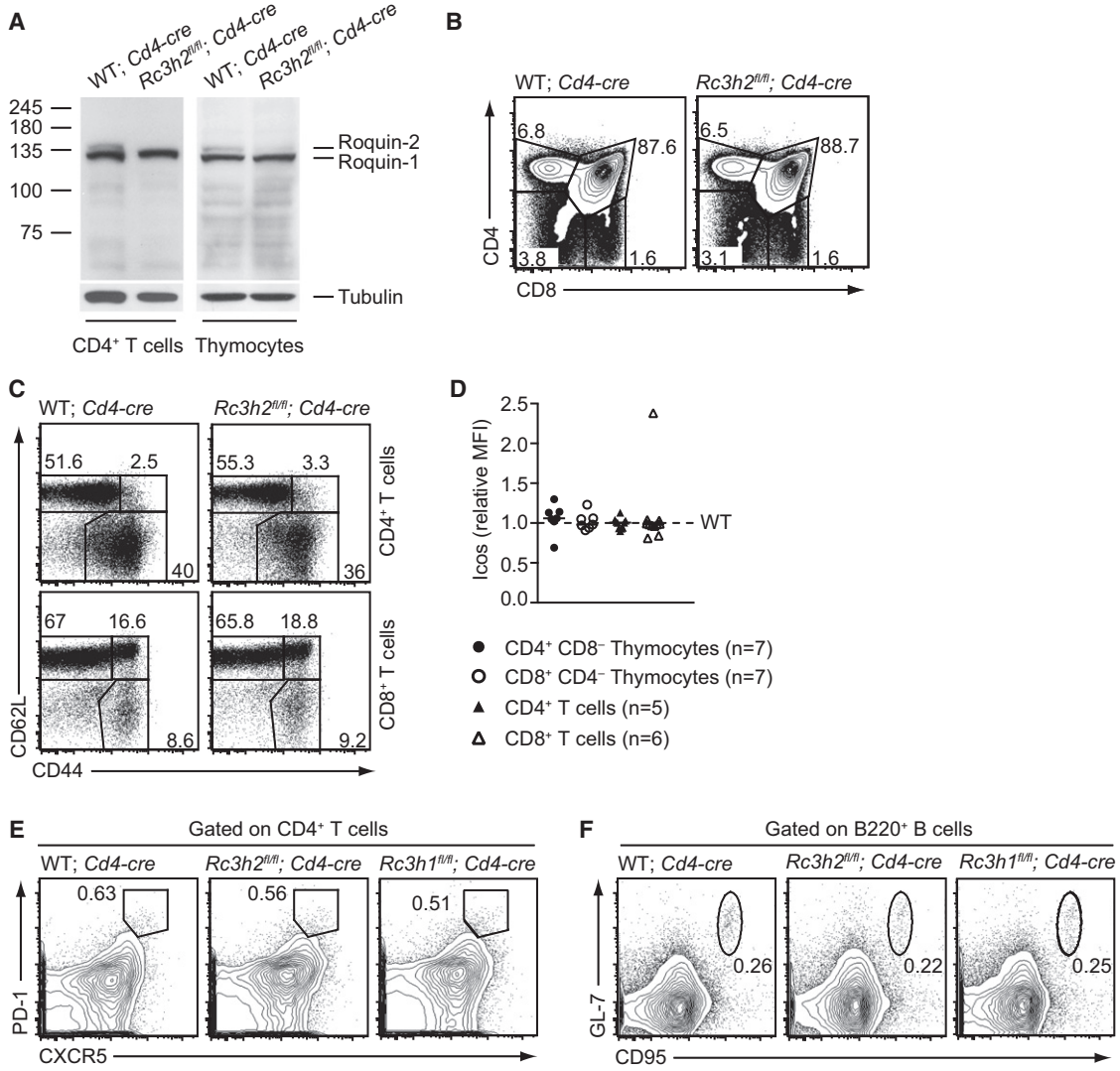

Figure 2. Deletion of *Rc3h2* in T Cells Does Not Affect Thymic Development, T Cell Differentiation, or Icos Expression

(A) Immunoblot analysis of Roquin-1 and Roquin-2 expression in $CD4^+$ T cells (left) or thymocytes (right). Protein expressions relative to WT are 12% for Roquin-2 and 97% for Roquin-1 in *Rc3h2*-deficient $CD4^+$ T cells and in thymocytes 63% for Roquin-2 and 108% for Roquin-1 (quantified by ImageJ). Representative flow cytometric analysis shows the frequencies of thymocyte subsets (B) or of $CD62L^{hi}$ $CD44^{lo}$, $CD62L^{lo}$ $CD44^{hi}$ or $CD62L^{hi}$ $CD44^{hi}$ splenic $CD4^+$, or $CD8^+$ T cells (C). (D) Relative median fluorescence intensity (MFI) of Icos in $CD4^+$ $CD8^-$ or $CD8^+$ $CD4^-$ thymocytes or splenic *Rc3h2*$^{fl/fl}$*; Cd4-cre* T cells, normalized to the respective *Cd4-cre* control T cell subset. Bars indicate medians.

(E and F) Representative contour plots showing proportions of splenic follicular helper T cells ($PD\text{-}1^{hi}$ $CXCR5^{hi}$) pregated on $CD4^+$ (E) and of germinal center B cells ($GL\text{-}7^{hi}$ $CD95^{hi}$) pregated on $B220^+$ (F). Genotypes are indicated in the figure, and data are representative for 3 experiments (A) or for 10 (B), 12 (C), and 5 (E–F) mice per genotype. See also Table S1.

naive $CD62L^{hi}$ $CD44^{lo}$ and a strongly increased frequency of activated $CD62L^{lo}$ $CD44^{hi}$ T cells. This phenotype was evident for $CD4^+$ and $CD8^+$ T cells and therefore different from *Rc3h1*$^{fl/fl}$*; Cd4-cre* mice, which did not show activation of $CD4^+$ T cells (Bertossi et al., 2011). In the $CD8^+$ T cell lineage, the activated phenotype was even more pronounced in the absence of both paralogs, with almost no naive and less $CD62L^{hi}$ $CD44^{hi}$ T cells (Figures 3C and 3D). We observed a significant decrease in absolute cell numbers for total $CD4^+$, naive $CD4^+$ and naive $CD8^+$ T cells, whereas $CD62L^{lo}$ $CD44^{hi}$ $CD8^+$ T cells were significantly increased (Figure 3D). Notably, no compensatory upregulation of Roquin-2 was detected in $CD4^+$ or $CD8^+$ T cells from *Rc3h1*-deficient mice or in $CD4^+$ T cells from *Rc3h1*$^{san/san}$ mice (Figures 3E and 3F; Figure S1F). The peripheral and thymic T regulatory (Treg) cell proportions of $CD4^+$ T cells were significantly increased, but this did not correspond with a significant increase in absolute numbers (Figures S2A and S2B). Taken together, *Rc3h1-2*$^{fl/fl}$*; Cd4-cre* mice exhibit the prominent phenotype of increased $CD8^+$ $CD62L^{lo}$ $CD44^{hi}$ cells seen in *Rc3h1*$^{fl/fl}$*; Cd4-cre* mice. In addition, they develop lymphadenopathy, splenomegaly, and the strongly increased $CD62L^{lo}$ $CD44^{hi}$ phenotype of $CD4^+$ and $CD8^+$ cells of the *Rc3h1*$^{san/san}$ mutant. These data

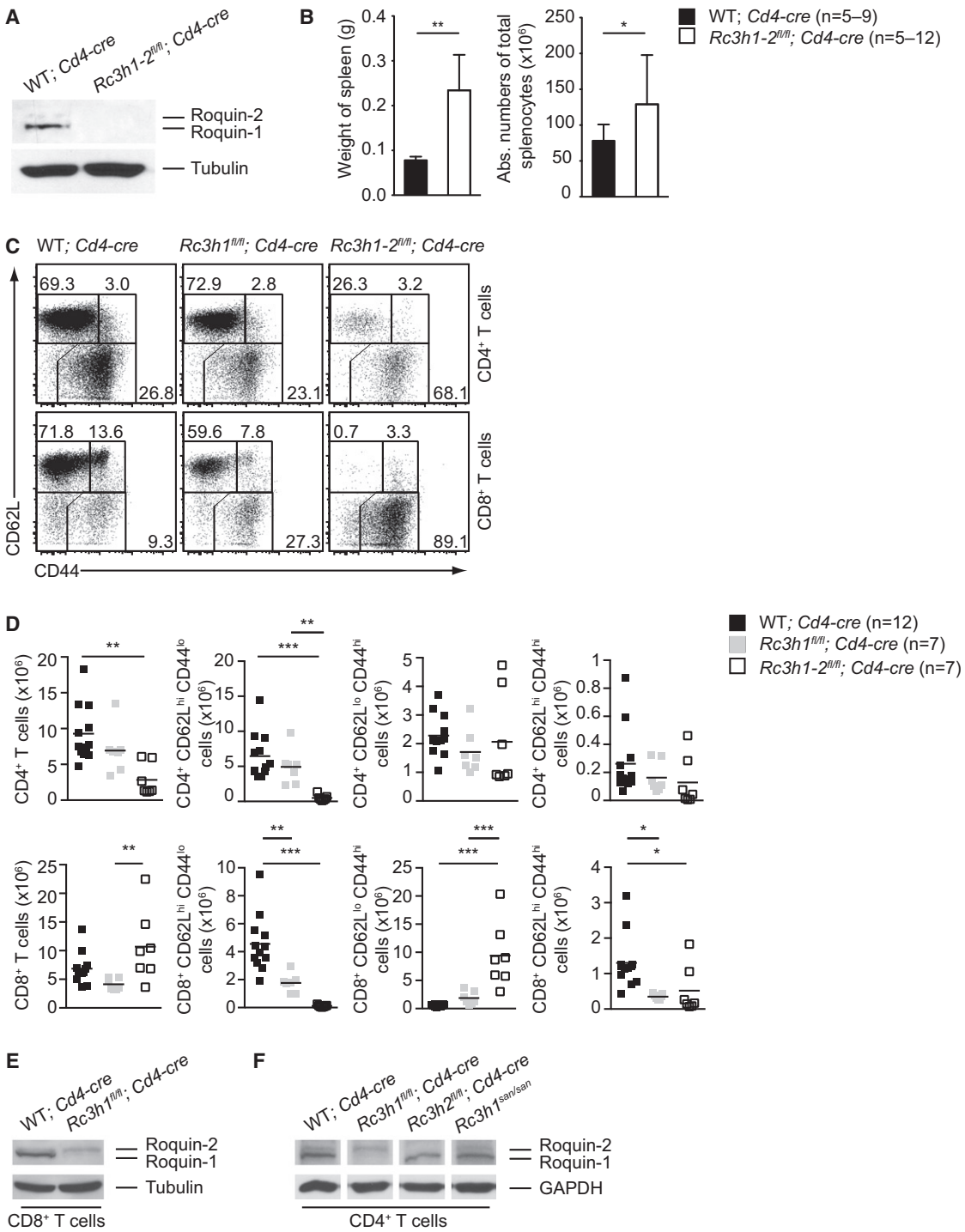

Figure 3. Combined Ablation of Roquin-1 and Roquin-2 in T Cells Reveals Functional Redundancy

(A) Immunoblot analysis confirming the ablation of Roquin-1 and Roquin-2 in $CD4^+$ T cells with tubulin as loading control.

(B) Spleen weight (left graph) and splenocyte number (right graph).

(C and D) Representative contour plots (C) and corresponding cells numbers (D) from $CD4^+$ (upper panel) or $CD8^+$ (lower panel) T cells, showing splenic $CD62L^{hi}$ $CD44^{lo}$, $CD62L^{lo}$ $CD44^{hi}$, or $CD62L^{hi}$ $CD44^{hi}$ T cells subsets.

(E and F) Bars indicate means. Immunoblot analysis of $CD8^+$ (E) or $CD4^+$ T cells (F) is shown. Statistical significances were calculated by Student's t test and Tukey's multiple comparisons test (*$p < 0.05$; **$p < 0.01$; ***$p < 0.001$). Genotypes are indicated in the figure, and data are represented as mean ± SD and representative for four (A), two (E), and 1–3 (F) experiments and 7–13 (C) mice per genotype and represented as mean ± SD. See also Figure S2.

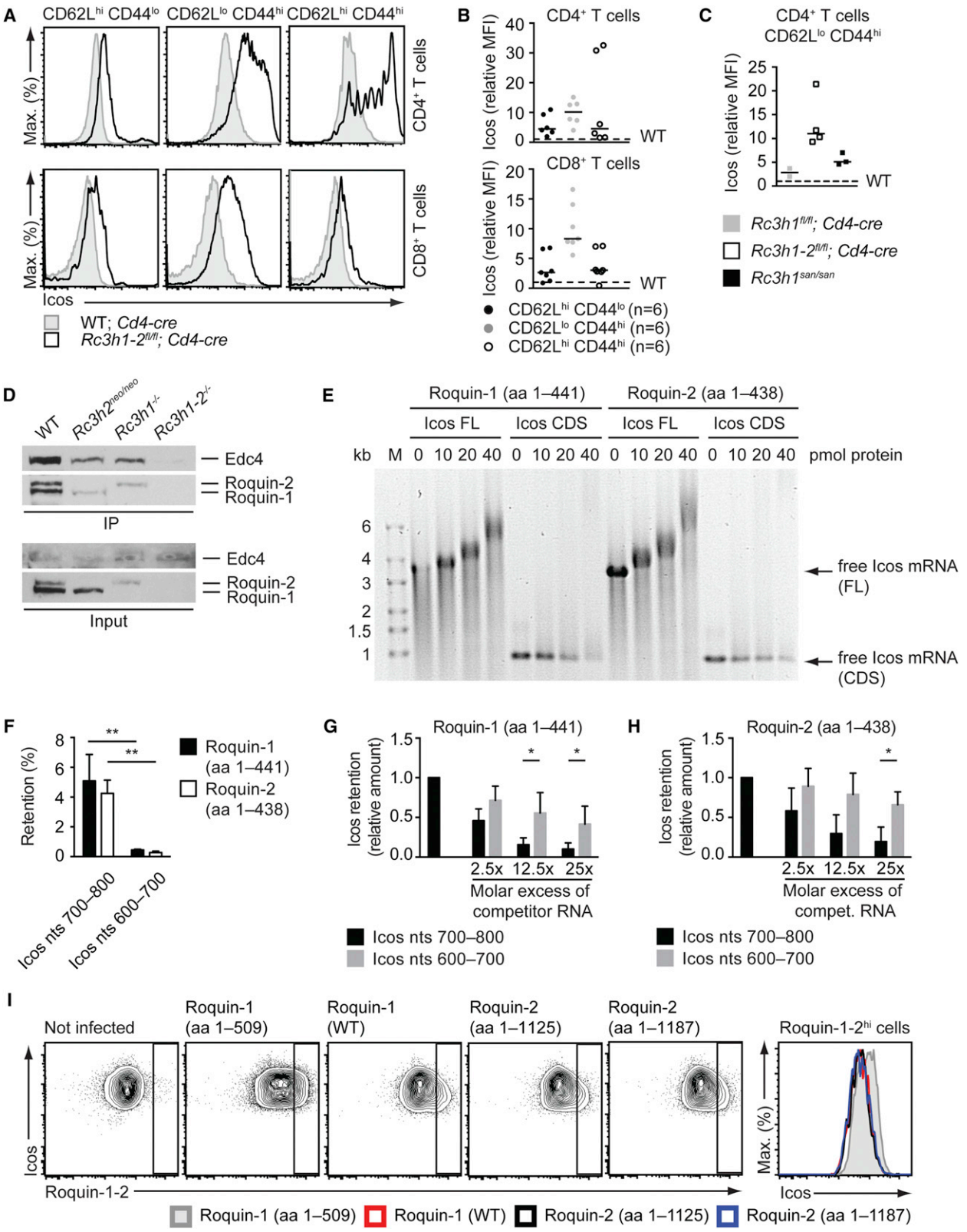

Figure 4. Both Roquin-1 and Roquin-2 Interact with Edc4 and Regulate Icos Expression

(A and B) Representative histograms (A) and relative median fluorescence intensity (MFI) (B) of Icos in CD62L^{hi} CD44^{lo}, CD62L^{lo} CD44^{hi} or CD62L^{hi} CD44^{hi} CD4^{+} (upper panel), or CD8^{+} (lower panel) *Rc3h1-2$^{fl/fl}$; Cd4-cre* T cells, normalized to Icos expression on *Cd4-cre* T cells. Bars indicate medians.

(legend continued on next page)

therefore suggest redundant functions of Roquin-1 and Roquin-2 in T cells.

Roquin-1 and Roquin-2 Redundantly Repress Icos mRNA

Icos expression in *Rc3h1-2*$^{fl/fl}$*; Cd4-cre* mice was increased on all T cells and much higher compared to *Rc3h1*$^{san/san}$ or *Rc3h1*$^{fl/fl}$*; Cd4-cre* mice (Figure 4A–4C). We therefore addressed the redundancy of both paralogs by comparing their association with Edc4, which is a cofactor of mRNA decapping and an interaction partner of Roquin-1 (Glasmacher et al., 2010). We used WT, single- and double-deficient MEF cells for anti-Roquin-1 and anti-Roquin-2 immunoprecipitation. Edc4 was equally well detected in immunoprecipitates from *Rc3h2*$^{neo/neo}$ or *Rc3h1*$^{-/-}$ MEF cell extracts (Figure 4D). Consistent with Edc4 interacting equally with both paralogs, the detection was maximal in immunoprecipitations from extracts of WT and absent in double-deficient MEFs (Figure 4D). We then assayed the recognition of Icos mRNA by amino-terminal fragments of Roquin-1 (aa 1–441) and Roquin-2 (aa 1–438) proteins. Electrophoretic mobility shift assays (EMSA) and filter binding assays showed similar characteristics of both proteins binding to the previously mapped *cis*-element (Icos nucleotides [nts] 700–800) (Glasmacher et al., 2010) (Figures 4E–4H). Roquin-1 and Roquin-2 proteins interacted much stronger with an Icos RNA-oligonucleotide harboring the *cis*-element (Icos nts 700–800) compared with another Icos RNA-oligonucleotide without the *cis*-element (Icos nts 600–700) (Figure 4F). The specificity of binding was confirmed by efficient competition with unlabeled Icos nts 700–800 and by much less efficient competition with Icos nts 600–700 (Figures 4G–4H). Finally, to prove functional redundancy we adenovirally introduced Roquin-1 protein or Roquin-2 isoforms into *Rc3h1*-deficient T cells. We employed a *CAG-CAR*$^{stop\text{-}fl}$ transgenic mouse (K.H., data not shown) (Figures S3A–S3C) that enabled the conditional expression of a truncated human coxsackie adenovirus receptor (CAR) (Wan et al., 2000). We generated *Rc3h1*$^{fl/fl}$*; CAG-CAR*$^{stop\text{-}fl}$*; Cd4-cre* mice and transduced CD4$^+$ T cells with adenoviruses expressing Roquin-1 and Roquin-2. In these experiments, both Roquin-2 isoforms (aa 1–1125 or aa 1–1187) downregulated Icos in a dose-dependent manner and their activity was undistinguishable from WT Roquin-1 protein, whereas an inactive mutant of Roquin-1 (aa 1–509) showed no effect (Figure 4I). Therefore, Roquin-1 and Roquin-2 proteins independently engage in the same molecular interactions with Edc4 protein and with Icos mRNA and can redundantly downregulate Icos expression in T cells.

Combined Loss of *Rc3h1* and *Rc3h2* Induces Differentiation of Tfh Cells

Rc3h1-2$^{fl/fl}$*; Cd4-cre* mice also exhibited strongly increased frequencies and absolute numbers of PD-1^{hi} CXCR5^{hi} Bcl6^{hi} Tfh cells compared to *Cd4-cre* control and *Rc3h1*$^{fl/fl}$*; Cd4-cre* mice in the absence of immunization (Figure 5A; Figure 5B). These Tfh cells were functional, as demonstrated by the concomitantly increased frequencies and numbers of germinal center B cells (Figures 5C and 5D). However, many of the *Rc3h1-2*$^{fl/fl}$*; Cd4-cre* animals had spleens with strongly reduced B cell counts and severe immune dysregulation (Figure 5E; Figure S4A). Unlike *Rc3h1*$^{san/san}$ mice, *Rc3h1-2*$^{fl/fl}$*; Cd4-cre* animals did not show spontaneous germinal center formation with the production of anti-nuclear antibodies (data not shown). By analyzing spleen sections by histology, we found a strong reduction in white pulp areas devoid of F4/80$^+$ macrophages (Figures S4B and S4C). This appeared to be due to unorganized or entirely absent follicular structures. Different from control spleens, B220$^+$ B cells were almost not detected and T cell areas were unorganized, with CD8$^+$ T cells being more affected than CD4$^+$ T cells (Figure 5E). In addition, MOMA-1$^+$ metallophilic macrophages appeared scattered and did not surround a follicle-like structure with a marginal zone (Figure 5E). The profound perturbations could result from altered communication of lymphocytes with the accessory cells in the spleen that is known to be essential for the formation and integrity of the follicle structure (Schneider et al., 2004). In fact, in the few follicle-like structures that could be found in the spleens of adult *Rc3h1-2*$^{fl/fl}$*; Cd4-cre* mice we noticed that the ER-TR7$^+$ reticular fibroblasts of the T cell zone appeared dispersed (Figure S4D), whereas follicular dendritic cells stained with anti-FDC-M1 could still be detected within a central network (Figure S4E). Although spleen sections from an only 3-week-old mouse were less affected, the frequency of intact primary follicles was also reduced (Figures S4F–S4J).

We then addressed whether adoptive transfer of polyclonal T cells with an acute deletion of *Rc3h1-2* alleles revealed spontaneous Tfh differentiation in an intact splenic environment (Figures 5F–5K). We achieved this by infecting cells with a cre-IRES-Thy1.1 encoding MSCV retrovirus, which allowed identification of transduced cells via Thy1.1 expression. The shared

(C) Relative median fluorescence intensity of Icos on CD62L^{lo} CD44^{hi} CD4$^+$ T cells of the indicated genotypes, normalized to Icos expression on *Cd4-cre* T cells. Bars indicate medians.
(D) Immunoprecipitation (IP) with magnetic beads coupled to an antibody, which recognizes both Roquin-1 and Roquin-2, of protein extracts from MEFs. Edc4, Roquin-1, and Roquin-2 proteins were detected by immunoblot analysis in IP and input.
(E) Electrophoretic mobility-shift assay with increasing amounts (0–40 pmol) of recombinant Roquin-1 (aa 1–441) or Roquin-2 (aa 1–438), incubated with in vitro-transcribed human Icos mRNA (1 pmol) either containing the 3′UTR (full-length, nts 1–2540) or lacking the 3′UTR (coding sequence [CDS], nts 1–600).
(F) Comparison of relative retention of Roquin-1 (aa 1–441) or Roquin-2 (aa 1–438) with human Icos fragments nts 700–800 or nts 600–700 by filter-binding assays.
(G and H) Filter-binding assays using 500 nM recombinant Roquin-1 (aa 1–441) (F) or Roquin-2 (aa 1–438) (G) incubated with human Icos nts 700–800 fragments and competed with cold human Icos nts 700–800 or nts 600–800 in molar excess.
(I) Adenoviral transduction of CD4$^+$ T cells from *Rc3h1*$^{fl/fl}$*; CAG-CAR*$^{stop\text{-}fl}$*; Cd4-cre* mice with adenovirus encoding an inactive Roquin-1 (aa 1–509), Roquin-1 WT, or two isoforms of Roquin-2 (aa 1–1125 or aa 1–1187). Surface staining of Icos and intracellular staining of Roquin-1 and −2 protein is shown in contour plots. The right graph shows a histogram overlay of Roquin-1^{hi} and Roquin-2^{hi} cells. All blots in (I) are pregated on CAR$^+$ cells. Statistical significances were calculated by Student's t test (*$p < 0.05$; **$p < 0.01$). Genotypes are indicated in the figure, and data are representative for six (A), two (C and D), and three (E and I) or means ± SD of three to four (F–H) experiments. See also Figure S3.

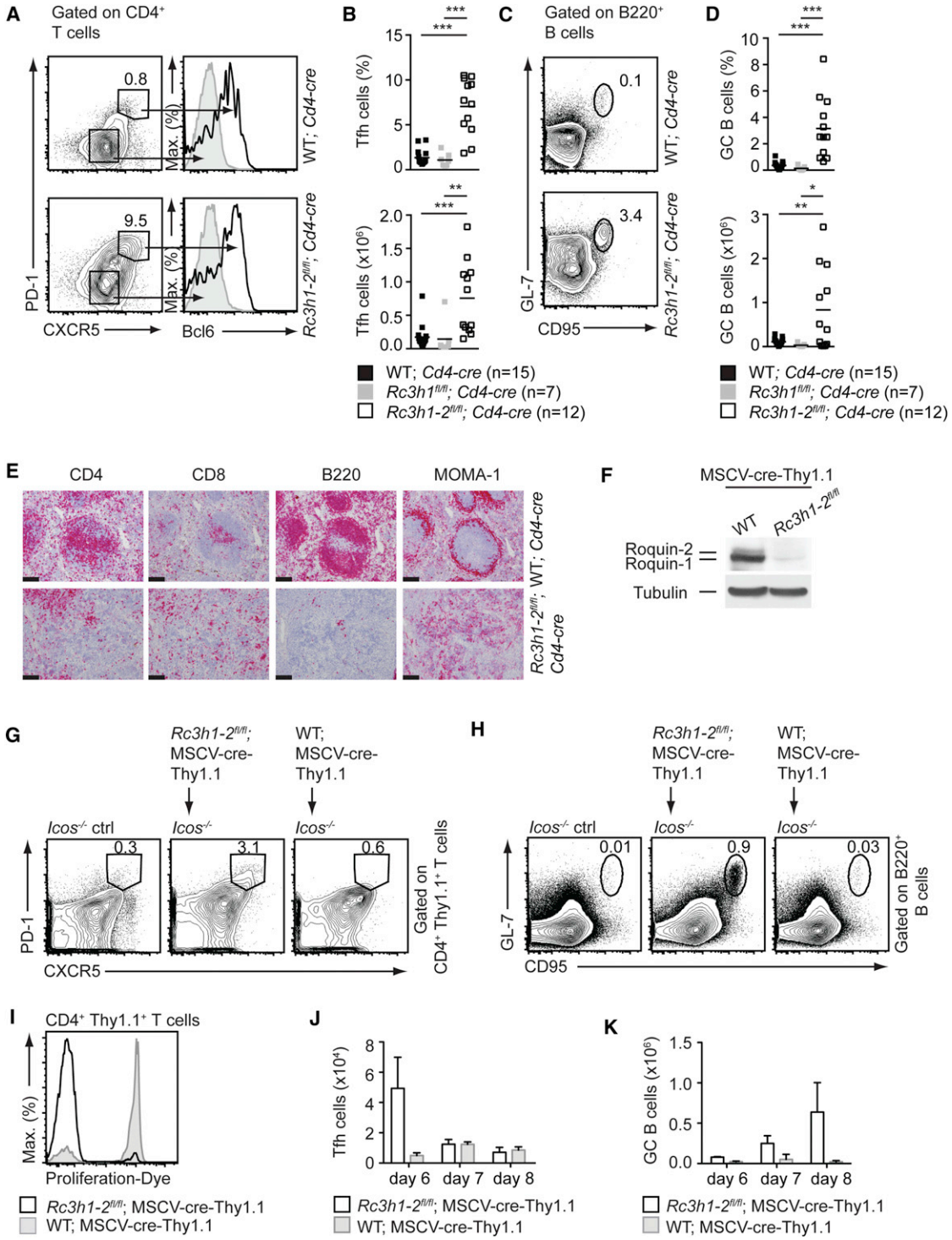

Figure 5. Combined Loss of *Rc3h1* and *Rc3h2* Drives Follicular T Helper (Tfh) Cell Differentiation

(A) Representative contour plots of splenic Tfh cells (PD-1^{hi} CXCR5^{hi}) pregated on CD4$^+$ T cells with histogram overlays showing Bcl6 expression.

(B) Percentage of Tfh cells (of CD4$^+$ T cells, upper panel) or Tfh cell numbers (lower panel). Bars indicate means.

(C) Representative contour plots of splenic germinal center B cells (GC B; GL-7^{hi} CD95^{hi}) pregated on B220$^+$ B cells, and (D) percentages of GC B cells (of B220$^+$ B cells, upper panel) or GC B cell numbers (lower panel). Bars indicate means.

(E) Consecutive cryosections from spleens, stained for CD4, CD8, B220, and MOMA-1 (scale bar represents 100 μm).

(F) Protein expression of Roquin-1 and Roquin-2 in cre-transduced CD4$^+$ T cells.

(G–I) Frequencies of Tfh cells (pregated on CD4$^+$ Thy1.1$^+$) on day 6 (G) or GC B cells (pregated on B220$^+$) on day 8 (H), as well as proliferation of CD4$^+$ Thy1.1$^+$ cells on day 6 (I) after transfer of MSCV-cre-Thy1.1-transduced WT or *Rc3h1-2*$^{fl/fl}$ cells (Th1-differentiated) into *Icos*$^{-/-}$ mice.

(legend continued on next page)

transitional stage of Th1 and Tfh cell differentiation (Nakayamada et al., 2011) prompted us to ablate *Rc3h1* and *Rc3h2* genes acutely within a 5 day Th1 cell culture before adoptive transfer into *Icos*-deficient hosts, which are impaired in endogenous Tfh cell generation (Choi et al., 2011). These experiments showed that acute loss of *Rc3h1-2* triggered Tfh cell differentiation of the transferred cells and induced host B cells to spontaneously undergo germinal center B cell differentiation (Figures 5G and 5H). $CD4^+$ T cells from *Rc3h1-2*$^{fl/fl}$ mice lost Roquin-1 and Roquin-2 protein expression five days after transduction (Figure 5F) and showed derepressed Icos expression (Figure S4K). Furthermore, IL-21 single- and IL-21 and IFN-γ double-producers were increased after restimulation of these cells with phorbol myristate acetate (PMA) and ionomycin (Figure S4L). On day 6 after transfer, $Thy1.1^+$ $CD4^+$ T cells that originated from *Rc3h1-2*$^{fl/fl}$ mice had proliferated vigorously (Figure 5I) and contained an elevated frequency and number of Tfh cells compared to WT $Thy1.1^+$ $CD4^+$ T cells (Figures 5G and 5J). The increased number of Tfh cells in the $Thy1.1^+$ $CD4^+$ T cells from *Rc3h1-2*$^{fl/fl}$ mice declined and reached similar Tfh cell numbers as WT cells within the next 2 days (Figure 5J). Six days after transfer of *Rc3h1-2*-deficient T cells, total B cell numbers moderately increased but declined until day 8, at which GC B cell numbers and frequencies were increased. This did not affect the frequency of $CD138^+$ plasma cells (data not shown; Figures 5H and 5K). Our data showed that the increased number of follicular helper T cells in *Rc3h1-2*$^{fl/fl}$*; Cd4-cre* mice was due to increased Tfh cell differentiation. The differentiation did not require ex vivo T cell activation because it was also observed after adoptive transfer of sorted naive $CD4^+$ T cells from *Rc3h1-2*$^{fl/fl}$*; Cd4-cre* mice (data not shown).

Roquin-1 and Roquin-2 Deficiency Induces Irf4 and the Alternative NF-κB Pathway

Having established that *Rc3h1-2*-deficient T cells undergo spontaneous Tfh cell differentiation in the absence of immunization, we tested expression of critical transcription factors of Tfh cells, among them Bcl6 and Irf4 (Bollig et al., 2012; Johnston et al., 2009; Kwon et al., 2009; Nurieva et al., 2009; Yu et al., 2009). We found increased amounts of Irf4 protein after acute deletion of *Rc3h1* and *Rc3h2* genes in Th1 cells as well as in $CD4^+$ T cells isolated from *Rc3h1-2*$^{fl/fl}$*; Cd4-cre* mice (Figures 6A–6D, top panels). Because Irf4 is a downstream target of NF-κB signaling, we tested spontaneous activation of the canonical (Figure 6B) or alternative pathway (Figure 6C) in *Rc3h1-2*-deficient Th1 cells. Enhanced IκBα degradation was not evident, but p65 protein amounts and phosphorylation were modestly increased. Phosphorylation of IκBα also appeared modestly elevated (Figure 6B). In contrast, mediators of the alternative pathway were strongly affected. Both p100 and Relb expression was increased, as was p100 processing to p52 (Figure 6C), which led to dramatic nuclear accumulation of p52 (Figure 6E). Also, $CD4^+$ T cells from *Rc3h1-2*$^{fl/fl}$*; Cd4-cre* mice displayed enhanced p100 processing and Irf4 protein amounts (Figure 6D). We hypothesized that spontaneous Irf4 and NF-κB activation in *Rc3h1-2*-deficient cells was a result of posttranscriptional derepression of one or more shared Roquin-1 and Roquin-2 targets in the alternative NF-κB pathway. We therefore tested mRNA expression of candidate genes in the NF-κB pathway by quantitative PCR (Figure 6F). During testing of *Ikkα*, *Ikkβ*, *Ikkγ*, *NIK*, *Ciap1*, *Ciap2*, *Traf2*, *Traf3*, and *Tradd* gene expression, we did not find an induction of these mRNAs in *Rc3h1-2*-deficient cells, whereas *Icos*, *Relb*, *Irf4*, and *Ox40* were increased (Figure 6F). Ox40 had been included as a candidate target gene because a small hairpin RNA (shRNA) that downregulated *Rc3h1* (Glasmacher et al., 2010) upregulated Ox40 expression (data not shown). Importantly, Ox40 has been shown to activate the NF-κB pathway (Murray et al., 2011) and was also increased on the protein level on the surface of $CD4^+$ T cells from *Rc3h1-2*$^{fl/fl}$*; Cd4-cre*, as well as *Rc3h1*$^{fl/fl}$*; Cd4-cre* but not *Rc3h2*$^{fl/fl}$*; Cd4-cre*, mice (Figure 6G). We then used an agonistic antibody to determine the effect of Ox40 stimulation in Th1 cells. Triggering of Ox40 clearly recapitulated alternative NF-κB activation in *Rc3h1-2*-deficient cells by inducing p100 processing to p52, but this stimulation alone was not sufficient to increase the Irf4 protein amounts (Figure 6H).

Ox40 is Posttranscriptionally Repressed by Roquin-1 and Roquin-2 Proteins

To find out whether Ox40 is a direct target, we tested binding of Roquin-1 and Roquin-2 proteins to the Ox40 mRNA. EMSA experiments showed that Ox40 and Icos mRNAs were similarly bound by Roquin-1 (Figure 7A) and Roquin-1 or Roquin-2 were indistinguishably bound to Ox40 mRNA (Figure 7B). In filter binding assays, the specific retention of the ^{32}P-labeled Ox40 3′UTR by Roquin-1 was effectively competed by an RNA-oligonucleotide with and, to a lesser extent, without the *cis*-element of the 3′UTR of Icos (compare Figure 7C Icos nts 700–800 with Icos nts 600–700). A similar binding and competition was observed for Roquin-2 (Figure 7D). We also demonstrated that Ox40 was downregulated in cells that overexpress Roquin-1 (Figures 7E and 7F). Specifically, we transduced *Rc3h1-2*-deficient MEF cells sequentially to express Ox40 and Roquin-1. Importantly, the downregulation depended on the expression of full-length Ox40 mRNA and WT Roquin-1 and did not occur when we expressed either Ox40 coding sequence with WT Roquin-1 or Ox40 full-length with the inactive mutant of Roquin-1 (aa 1–509) (Figure 7E). Finally, by using adenoviral transduction of $CD4^+$ T cells from *Rc3h1*$^{fl/fl}$*; CAG-CAR*$^{stop\text{-}fl}$*; Cd4-cre* mice, we demonstrated that endogenous Ox40 surface expression was downregulated to a similar extent by a comparable overexpression of the Roquin-1 protein or either isoform of Roquin-2 (Figure 7F). By this we present Ox40 as another posttranscriptional target of Roquin-1 and Roquin-2, which might therefore contribute to the observed activation of T cells and the increased Tfh cell differentiation, as well as the development of autoimmune disease.

(J and K) Cell numbers of Tfh (J) or GC B (K) cells at day 6, 7, and 8 after transfer. Statistical significances were calculated by Tukey's multiple comparisons test (*$p < 0.05$; **$p < 0.01$; ***$p < 0.001$). Genotypes are indicated in the figure and data are representative for 12 (A–D) and more than three (E) mice per genotype, and six (F) or five (G–K) experiments with two (G, H, J, K) and three (I) mice per group. Data are represented as mean ± SD. See also Figure S4.

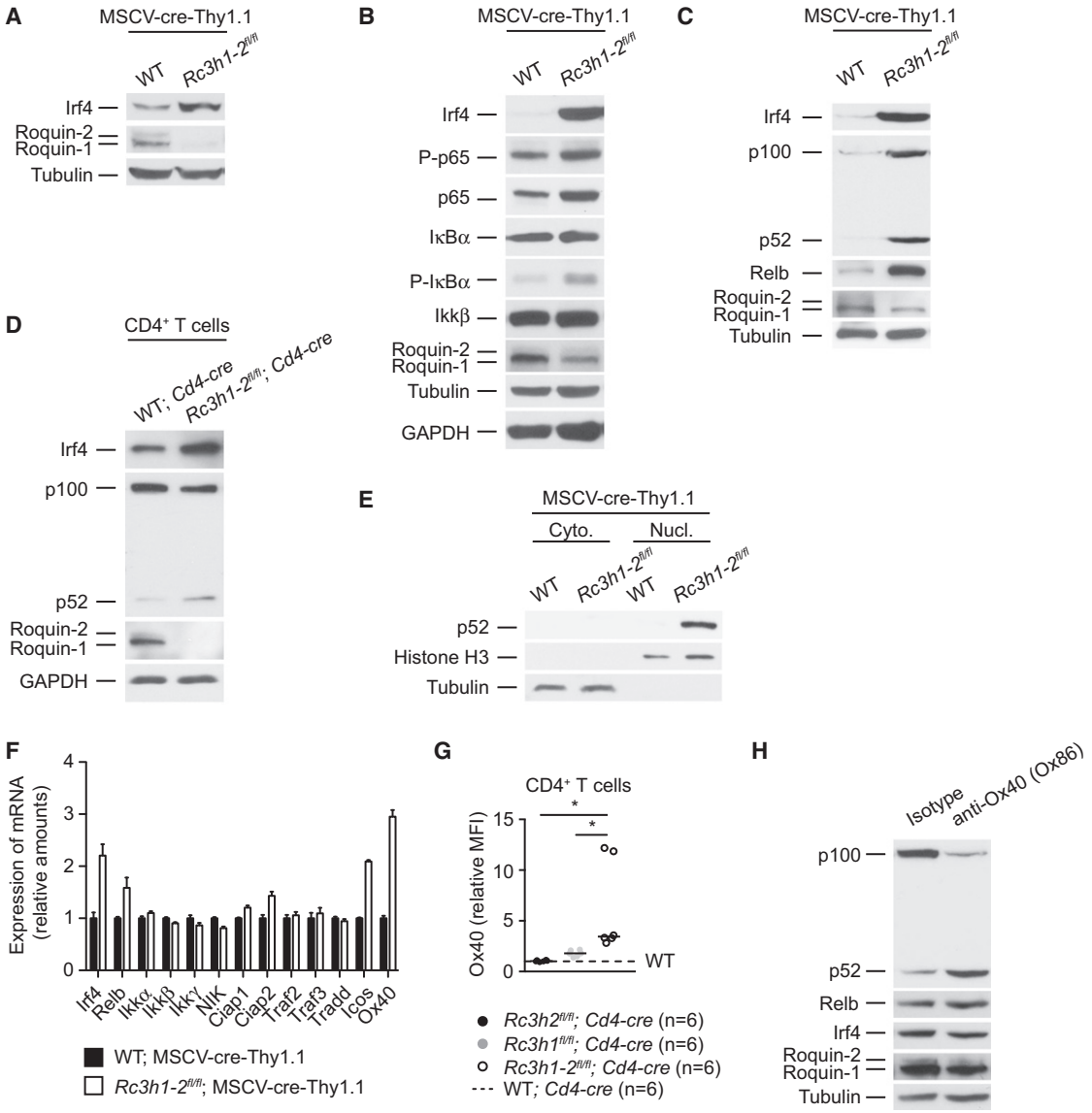

Figure 6. *Rc3h1-2* Deletion Elevates Irf4 and Ox40 Expression and Leads to Activation of the NF-κB Pathway

Immunoblot analysis of protein lysates from WT or *Rc3h1-2*$^{fl/fl}$ CD4$^+$ T cells after cre-transduction, showing Irf4 expression (A) and factors involved in the canonical (B) or alternative NF-κB pathway (C), each representing an independent experiment.

(D) Immunoblot analysis of purified CD4$^+$ T cells, showing factors of the noncanonical NF-κB pathway.

(E) Immunoblot analysis of cytoplasmic and nuclear extracts from WT or *Rc3h1-2*$^{fl/fl}$ CD4$^+$ T cells after cre-transduction. Data are representative for four (D) and three (E) experiments.

(F) Quantitative PCR analysis of factors involved in NF-κB signaling. Data are representative for three biological replicates from WT or *Rc3h1-2*$^{fl/fl}$ CD4$^+$ T cells after cre-transduction.

(G) Relative MFI of Ox40 in Roquin-1- and Roquin-2-deficient CD4$^+$ T cells normalized to *Cd4-cre* T cells. Bars show medians.

(H) Immunoblot of Th1-differentiated CD4$^+$ T cell lysates from C57BL/6 mice, treated with 10 μg/ml isotype control antibody or anti-Ox40 (OX86) for 3 days, showing factors of the alternative NF-κB pathway. Genotypes are indicated in the figure, and data are representative for three experiments. Statistical significances were calculated by Tukey's multiple comparisons test (*$p < 0.05$). Data are represented as mean ± SD. See also Table S2.

DISCUSSION

In this study we defined Ox40 as a new target of Roquin-1 and Roquin-2 through direct binding and 3′UTR-dependent post-transcriptional repression. Combined ablation of *Rc3h1* and *Rc3h2* in T cells induced the expression of Ox40 and the activation of the alternative NF-κB pathway, which was also observed in WT cells after stimulation of Ox40. In addition, we found that *Rc3h1-2*-deficient T cells contained elevated expression of the NF-κB target genes *Relb* and *Irf4* (Basak et al., 2008; Grumont and Gerondakis, 2000; Sasaki et al., 2008). Although stimulation of Ox40 alone did not induce Irf4, we nevertheless think that

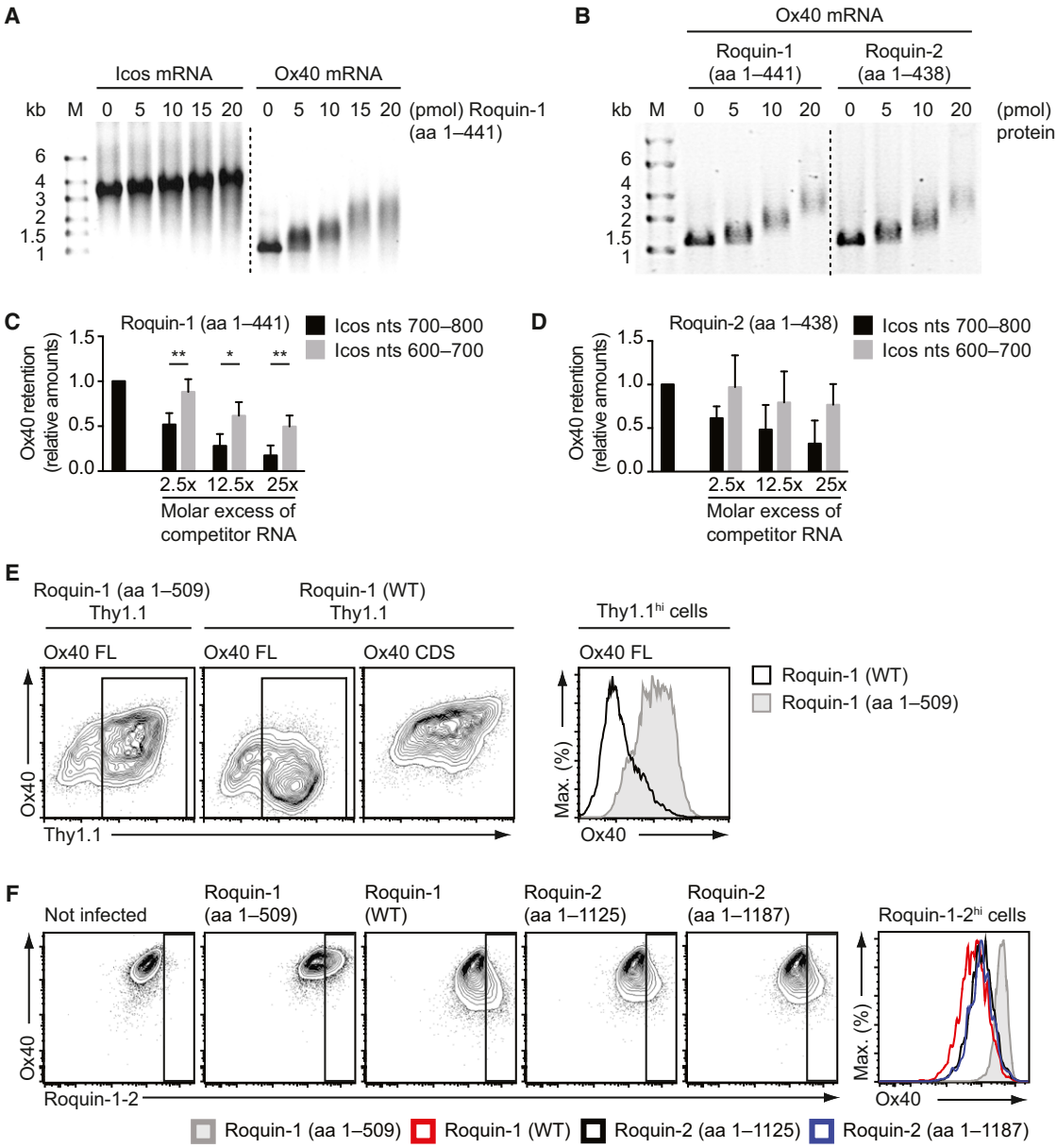

Figure 7. Roquin-1 and Roquin-2 Redundantly Control Ox40 Expression

(A and B) EMSA performed with (A) 0–20 pmol of recombinant Roquin-1 (aa 1–441) protein, incubated with 1 pmol of in vitro-transcribed human Icos (full-length) or mouse Ox40 (full-length) mRNA or (B) with 1 pmol mouse Ox40 (full-length) mRNA and 0–20 pmol Roquin-1 (aa 1–441) or Roquin-2 (aa 1–438).

(C and D) Filter-binding assay that used recombinant Roquin-1 (aa 1–441) (C) or Roquin-2 (aa 1–438) (D) incubated with mouse Ox40 3′UTR and competed with cold human Icos nts 700–800 or with cold human Icos nts 600–800 in molar excess as indicated.

(E) Representative contour blots and histogram overlay (right) of Ox40 and Roquin-1 (as Thy1.1) in *Rc3h1-2*-deficient MEFs, transduced with a retrovirus encoding full-length (FL) or coding sequence (CDS) Ox40 mRNA, and superinfected with a retrovirus encoding IRES-Thy1.1 with inactive Roquin-1 (aa 1–509) or WT Roquin-1.

(F) Contour plots showing surface Ox40 and intracellular Roquin-1 and Roquin-2 expression after adenoviral transduction of $CD4^+$ T cells from *Rc3h1*$^{fl/fl}$*; CAG-CAR*$^{stop\text{-}fl}$*; Cd4-cre* mice with an inactive Roquin-1 (aa 1–509), Roquin-1 WT, or two isoforms of Roquin-2 (aa 1–1125 or aa 1–1187). The right graph shows a histogram overlay of Roquin-1^{hi} and Roquin-2^{hi} cells. All plots in (F) are pregated on CAR^+ cells. Statistical significances were calculated by Student's t test (*$p < 0.05$; **$p < 0.01$). Data are representative for five (A), two (B), and three (E and F) or the means ± SD of three to four (C and D) experiments.

cellular Irf4 amounts are increased as a result of Ox40 in conjunction with other signals in *Rc3h1-2*-deficient T cells. However, we cannot rule out Irf4 as a direct target of Roquin-1 and Roquin-2. Increased Irf4 activity might augment Tfh cell numbers because *Irf4*-deficient T cells are greatly impaired in this differentiation program (Bollig et al., 2012; Kwon et al., 2009). Irf4 can also directly bind the promoter of *Icos* and induce its expression (Zheng et al., 2009), which could additionally explain the

exceedingly high Icos surface expression on *Rc3h1-2*-deficient T cells. Interestingly, the Irf4-binding protein Def6 has been shown to negatively regulate Irf4 transcriptional activity (Chen et al., 2008), and deficiency of Def6 correlates with systemic lupus-like autoimmunity (Fanzo et al., 2006). Similarly, Ox40 has been implicated in a large number of autoimmune diseases (Croft, 2010), whereas deletion of Ox40 together with CD30 rescues lethal autoimmunity in *Foxp3*-deficient mice (Gaspal et al., 2011).

Both Icos and Ox40 are important for the survival of effector T cells (Simpson et al., 2010; Weinberg, 2010). Constitutive Ox40 triggering through transgenic expression of the Ox40 ligand on T cells leads to massive induction of effector memory $CD4^+$ but not $CD8^+$ T cells (Murata et al., 2002). Ox40 is linked to Tfh cell development because transgenic Ox40L overexpression on dendritic cells increases the appearance of $CD4^+$ T cells with a $CD62L^{lo}$ phenotype, which accumulate in germinal centers after immunization (Brocker et al., 1999). In a very recent publication, IFN-γ has been proposed to be a potential new target of Roquin-1 and involved in the accumulation of short-lived effector $CD8^+$ T cells (SLEC) with enhanced effector function in san/san mice (Chang et al., 2012). However, the so far presented evidence cannot rule out indirect stabilization of IFN-γ mRNA in SLECs from san/san mice. Such stabilization of the mRNA of IFN-γ and other cytokines has been reported in the context of Ox40 stimulation (Mestas et al., 2005). Ox40 activates NF-κB and overlaps with downstream Icos signaling in the activation of PI3K (Gigoux et al., 2009; So et al., 2011). Remarkably, the extent of PI3K activation during immunization has been shown to determine the magnitude of the germinal center reaction (Rolf et al., 2010). Our findings therefore imply that both costimulatory pathways of Icos and Ox40 work in a redundant and cooperative manner to enhance Tfh cell differentiation in *Rc3h1-2*-deficient $CD4^+$ T cells.

We showed that combined *Rc3h1* and *Rc3h2* deficiency in T cells led to spontaneous Tfh and GC B cell differentiation in the absence of immunization but did not induce anti-nuclear antibodies. This can be due to several reasons. The observed changes in san/san mice might require the presence of the mutation in cells outside of the T cell compartment. On the other hand, we propose that the profound perturbation of the splenic microarchitecture might no longer permit progression toward a lupus-like disease. At this point we do not know which *trans*-acting factor produced by *Rc3h1-2*-deficient T cells interferes with the follicle organization.

In light of the determined functional redundancy, it was remarkable that the five-times lower expression of Roquin-2 compared to Roquin-1 in $CD4^+$ T cells did not correlate with the functional impact of the protein in the individual mouse models. This was not only true for Icos regulation but also for the control of effector memory T cell and Tfh cell phenotypes. Notably, Roquin-2 protein was not upregulated in *Rc3h1*-deficient T cells or in $CD4^+$ T cells from $Rc3h1^{san/san}$ mice. Considering these mouse models, we find that (1) even very low amounts of Roquin-2 in $CD4^+$ T cells were able to functionally compensate for most of the loss of function due to ablation of *Rc3h1*. (2) The same amount of Roquin-2 protein in T cells that also express the Roquin-1^{san} protein was much less able to complement the hypomorphic function of Roquin-1^{san} in posttranscriptional gene regulation (Vinuesa et al., 2005; Yu et al., 2007), and (3) deletion of *Rc3h2* in T cells that express WT Roquin-1 had no obvious effect. (4) In contrast however, we found that combined deletion of *Rc3h2* and *Rc3h1* dramatically increased Icos and Ox40 surface expression and massively induced Tfh cell differentiation as well as effector memory phenotypes in $CD4^+$ and $CD8^+$ T cells. We therefore conclude that the redundant activity of Roquin-2 must be inhibited in the presence of Roquin-1^{san} or Roquin-1 WT proteins. The nature of this inhibition is unknown but might involve dominant-negative effects, competition for a shared and limiting factor, or negative feedback regulation.

The evolutionary advantage of *Rc3h1* and *Rc3h2* gene duplication can be seen in a safe guard system that protects us from autoimmunity and tumorigenesis. It might also involve a so-far undiscovered diversification of both paralogs, considering the postnatal lethality of the individual genetically ablated mice. Our present study reveals that in T cells, Roquin-1 and Roquin-2 proteins redundantly restrict T cell activation and costimulation via Icos and Ox40 to prevent inappropriate Tfh cell differentiation.

EXPERIMENTAL PROCEDURES

Mice

C57BL/6 mice were from Taconic Farms, and $Rc3h1^{san}$ mice (EM:02168) were obtained from EMMA consortia. All animals were housed in a pathogen-free barrier facility in accordance with the Helmholtz Zentrum München institutional, state, and federal guidelines.

Cell Isolation, Culture, and Stimulation

Mouse embryonic fibroblasts were grown in DMEM with 10% (vol/vol) FCS, penicillin-streptomycin (1,000 U/ml), and HEPES (10 mM), pH 7.4. $CD4^+$ T cells were isolated from spleens and lymph nodes by using CD4 dynabeads and detachabeads (Invitrogen) according to the manufacturer's protocol. For Th1 differentiation, cells were stimulated on precoated plates (goat anti-hamster IgG; MP biochemicals) with anti-CD3 (145-2C11; 0.1–0.25 μg/ml), anti-CD28 (37N; 1–2.5 μg/ml), anti-IL-4 (IIB11; 10 μg/ml), and recombinant IL-12 (10 ng/ml; BD Biosciences). Anti-Ox40 (Ox86, 10 μg/ml) or isotype antibody (rat IgG, 10 μg/ml, eBioscience) was used for NF-κB activation. Antibodies were produced in-house unless otherwise stated. Two days after stimulation, $CD4^+$ T cells were cultured in the presence of recombinant hIL-2 (20 U/ml, ProleukinS, Novartis).

Virus Production and Transduction

Type 5 replication-deficient adenovirus was produced by transfection with JetPI (Polyplus) transfectant and amplified in HEK293A cells. Cells were harvested and dissolved in 800 μl medium, followed by three freeze-thaw cycles. We incubated 2×10^6 $CD4^+$ CAR^+ T cells with 100–300 μl virus-supernatant for 2 hr at 37°C. Retrovirus production and retroviral transduction for in vitro deletion and transfer is described in Supplemental Information.

Coimmunoprecipitation, Nuclear Fractionation, and Immunoblotting

For coimmunoprecipitations (coIP), mouse embryonic fibroblasts were lysed on ice in lysis buffer (20 mM Tris-HCl, pH 7.5, 150 mM NaCl, 0.25% [vol/vol] Nonidet-P40, 1.5 mM $MgCl_2$, protease inhibitor mix without EDTA [Roche], and 1 mM dithiothreitol), were shock frozen, thawed, and cleared by centrifugation (10,000 g, 4°C, 10 min). Anti-Rc3h1-2 (Q4-2, in-house production) coupled to magnetic beads (Invitrogen) was incubated for 4 hr at 4°C with lysates. Beads were washed three times with lysis buffer and boiled in SDS loading buffer at 95°C for 5 min, and the supernatant was used for immunoblotting. For cytoplasmic and nuclear fractionation, cells were resuspended in 200 μl buffer A (10 mM HEPES, pH 7.9, 10 mM KCl, 0.1 mM EDTA, 1 mM

dithiothreitol, protease inhibitor mix without EDTA [Roche]), incubated 15 min on ice, and dounced 10 times. After centrifugation (10 min, 4°C, 20,000 g), the supernatant was used for immunoblotting and the pellet was washed two times with buffer A. The nuclear and cell pellets were generally lysed for 15 min on ice in RIPA buffer (20 mM Tris-HCl, pH 7.5, 150 mM NaCl, 1% Triton X-100, 1% sodium deoxycholate, 0.1% SDS, 5 mM EDTA, 1 mM dithiothreitol, protease inhibitor mix without EDTA [Roche]). After one freeze-thaw cycle and centrifugation immunoblotting was performed by standard protocols with commercial antibodies (see Supplemental Information). For Roquin-1 and Roquin-2 recognition we generated monoclonal antibodies (3F12) via immunization of rats using Roquin-1 (aa 1–441) protein.

Flow Cytometry and Intracellular Staining

Single-cell suspensions of thymus and spleen were preincubated with Fc-block (CD16/31; 2.4G2; in-house production) in staining buffer (PBS, 2% FBS, 2 mM EDTA) for 10 min at 4°C and stained with antibodies for 20 min at 4°C. All antibodies used, including those in Table S1 and Figures S3 and S4 are described in Supplemental Information. Stainings of CXCR5, Bcl6, Foxp3, and Roquin-1 and Roquin-2 are described in Supplemental Information. Samples were acquired on a FACSCalibur, LSRII, or LSRFortessa (BD Biosciences) and analyzed with FlowJo software (Tree Star).

Protein Purification

Roquin-1 (aa 1–441) was purified as described (Glasmacher et al., 2010) and Roquin-2 (aa 1–438) was expressed from the vector pETM-11 in *E. coli* Rosetta2 (DE3) and purified by affinity chromatography (HiTrap Chelating column) and size exclusion chromatography (16/60 HiLoad Superdex 200 column). The purification buffer was 50 mM Tris-HCl pH 8.0, 300 mM NaCl, 0.01% (v/v) 1-thioglycerol.

In Vitro RNA Transcription

RNA was transcribed as described (Glasmacher et al., 2010).

Electrophoretic Mobility Shift Assay

Shift assays were performed as described (Glasmacher et al., 2010) with the following binding buffer: 150 mM NaCl, 20 mM HEPES, pH 7.4, 1 mM $MgCl_2$, and 1 mM dithiothreitol, adjusted to 16% (vol/vol) glycerol.

Filter Binding Assay

On the basis of equimolar amounts of DNA oligonucleotides (Ox40 3′UTR nts 999–1142 [NM_011659], Icos nts 600–700, Icos nts 700–800 [NM_012092.3]), RNA was transcribed by using T7 RNA polymerase (Agilent Technologies) in the presence of α-^{32}P-UTP. After the binding reaction of 500 nM recombinant Roquin-1 (aa 1–441) or Roquin-2 (aa 1–438) and RNA (30 min at 37°C in 20 mM HEPES, pH 7.4, 150 mM NaCl, 1 mM $MgCl_2$, 1 mM dithiothreitol, and 1 μg/μl BSA), the samples were applied onto nitrocellulose filters in a dot blot device. After five washing steps, protein-bound RNA was quantified by using a phosphoimager and normalized to RNA spotted onto nitrocellulose without washing to obtain the percentage of retention. For competition experiments, unlabeled RNA was added to the binding reaction.

Quantitative Real-Time PCR

RNA was isolated from Th1 T cell lysates with TRIzol (Life Technologies) and reverse transcribed with the Quantitect kit (QIAGEN). Quantitative PCR assays were run on a Light Cycler 480II device with the Light Cycler 480 SW 1.5 software. Primers and universal probes (Roche) are given in Table S2.

Statistical Analysis

Statistical analyses were performed with GraphPad Prism 5.0d and p values were calculated by Student's t test, one-way ANOVA, or Tukey's multiple comparisons test.

SUPPLEMENTAL INFORMATION

Supplemental Information includes four figures, two tables, and Supplemental Experimental Procedures and can be found with this article online at http://dx.doi.org/10.1016/j.immuni.2012.12.004.

ACKNOWLEDGMENTS

We would like to thank C. Wolf for expert technical assistance, C. Vahl for help with cell sorting, and R. Kroczek (Robert Koch Institute, Berlin, Germany) for *Icos*$^{-/-}$ mice. The PBS57-loaded CD1d tetramer was obtained through the National Institutes of Health Tetramer Facility. This work was supported by an ERC grant to V.H., the SFB1054 (TP-A03 to V.H.), a grant from the Thyssen foundation to V.H. and M.S.-S., a DFG Emmy Noether grant to M.S.-S., and by a grant of the FP7 program of the European Commission (EU) EUCOMMTOOLS (HEALTH-F4-2010-261492) to W.W. G.A.H and K.H. were supported by fellowships from Boehringer Ingelheim.

Received: July 31, 2012
Accepted: December 6, 2012
Published: April 11, 2013

REFERENCES

Ansel, K.M., McHeyzer-Williams, L.J., Ngo, V.N., McHeyzer-Williams, M.G., and Cyster, J.G. (1999). In vivo-activated CD4 T cells upregulate CXC chemokine receptor 5 and reprogram their response to lymphoid chemokines. J. Exp. Med. *190*, 1123–1134.

Athanasopoulos, V., Barker, A., Yu, D., Tan, A.H., Srivastava, M., Contreras, N., Wang, J., Lam, K.P., Brown, S.H., Goodnow, C.C., et al. (2010). The ROQUIN family of proteins localizes to stress granules via the ROQ domain and binds target mRNAs. FEBS J. *277*, 2109–2127.

Basak, S., Shih, V.F., and Hoffmann, A. (2008). Generation and activation of multiple dimeric transcription factors within the NF-kappaB signaling system. Mol. Cell. Biol. *28*, 3139–3150.

Baumjohann, D., Okada, T., and Ansel, K.M. (2011). Cutting Edge: Distinct waves of BCL6 expression during T follicular helper cell development. J. Immunol. *187*, 2089–2092.

Bauquet, A.T., Jin, H., Paterson, A.M., Mitsdoerffer, M., Ho, I.C., Sharpe, A.H., and Kuchroo, V.K. (2009). The costimulatory molecule ICOS regulates the expression of c-Maf and IL-21 in the development of follicular T helper cells and TH-17 cells. Nat. Immunol. *10*, 167–175.

Bertossi, A., Aichinger, M., Sansonetti, P., Lech, M., Neff, F., Pal, M., Wunderlich, F.T., Anders, H.J., Klein, L., and Schmidt-Supprian, M. (2011). Loss of Roquin induces early death and immune deregulation but not autoimmunity. J. Exp. Med. *208*, 1749–1756.

Betz, B.C., Jordan-Williams, K.L., Wang, C., Kang, S.G., Liao, J., Logan, M.R., Kim, C.H., and Taparowsky, E.J. (2010). Batf coordinates multiple aspects of B and T cell function required for normal antibody responses. J. Exp. Med. *207*, 933–942.

Bollig, N., Brüstle, A., Kellner, K., Ackermann, W., Abass, E., Raifer, H., Camara, B., Brendel, C., Giel, G., Bothur, E., et al. (2012). Transcription factor IRF4 determines germinal center formation through follicular T-helper cell differentiation. Proc. Natl. Acad. Sci. USA *109*, 8664–8669.

Brocker, T., Gulbranson-Judge, A., Flynn, S., Riedinger, M., Raykundalia, C., and Lane, P. (1999). CD4 T cell traffic control: in vivo evidence that ligation of OX40 on CD4 T cells by OX40-ligand expressed on dendritic cells leads to the accumulation of CD4 T cells in B follicles. Eur. J. Immunol. *29*, 1610–1616.

Chang, P.P., Lee, S.K., Hu, X., Davey, G., Duan, G., Cho, J.H., Karupiah, G., Sprent, J., Heath, W.R., Bertram, E.M., and Vinuesa, C.G. (2012). Breakdown in repression of IFN-γ mRNA leads to accumulation of self-reactive effector CD8+ T cells. J. Immunol. *189*, 701–710.

Chen, Q., Yang, W., Gupta, S., Biswas, P., Smith, P., Bhagat, G., and Pernis, A.B. (2008). IRF-4-binding protein inhibits interleukin-17 and interleukin-21 production by controlling the activity of IRF-4 transcription factor. Immunity *29*, 899–911.

Choi, Y.S., Kageyama, R., Eto, D., Escobar, T.C., Johnston, R.J., Monticelli, L., Lao, C., and Crotty, S. (2011). ICOS receptor instructs T follicular helper cell versus effector cell differentiation via induction of the transcriptional repressor Bcl6. Immunity *34*, 932–946.

Croft, M. (2010). Control of immunity by the TNFR-related molecule OX40 (CD134). Annu. Rev. Immunol. *28*, 57–78.

Crotty, S. (2011). Follicular helper CD4 T cells (TFH). Annu. Rev. Immunol. *29*, 621–663.

Fanzo, J.C., Yang, W., Jang, S.Y., Gupta, S., Chen, Q., Siddiq, A., Greenberg, S., and Pernis, A.B. (2006). Loss of IRF-4-binding protein leads to the spontaneous development of systemic autoimmunity. J. Clin. Invest. *116*, 703–714.

Gaspal, F., Withers, D., Saini, M., Bekiaris, V., McConnell, F.M., White, A., Khan, M., Yagita, H., Walker, L.S., Anderson, G., and Lane, P.J. (2011). Abrogation of CD30 and OX40 signals prevents autoimmune disease in FoxP3-deficient mice. J. Exp. Med. *208*, 1579–1584.

Gigoux, M., Shang, J., Pak, Y., Xu, M., Choe, J., Mak, T.W., and Suh, W.K. (2009). Inducible costimulator promotes helper T-cell differentiation through phosphoinositide 3-kinase. Proc. Natl. Acad. Sci. USA *106*, 20371–20376.

Glasmacher, E., Hoefig, K.P., Vogel, K.U., Rath, N., Du, L., Wolf, C., Kremmer, E., Wang, X., and Heissmeyer, V. (2010). Roquin binds inducible costimulator mRNA and effectors of mRNA decay to induce microRNA-independent post-transcriptional repression. Nat. Immunol. *11*, 725–733.

Grumont, R.J., and Gerondakis, S. (2000). Rel induces interferon regulatory factor 4 (IRF-4) expression in lymphocytes: modulation of interferon-regulated gene expression by rel/nuclear factor kappaB. J. Exp. Med. *191*, 1281–1292.

Hoefig, K.P., and Heissmeyer, V. (2008). MicroRNAs grow up in the immune system. Curr. Opin. Immunol. *20*, 281–287.

Hu, Y.L., Metz, D.P., Chung, J., Siu, G., and Zhang, M. (2009). B7RP-1 blockade ameliorates autoimmunity through regulation of follicular helper T cells. J. Immunol. *182*, 1421–1428.

Ise, W., Kohyama, M., Schraml, B.U., Zhang, T., Schwer, B., Basu, U., Alt, F.W., Tang, J., Oltz, E.M., Murphy, T.L., and Murphy, K.M. (2011). The transcription factor BATF controls the global regulators of class-switch recombination in both B cells and T cells. Nat. Immunol. *12*, 536–543.

Johnston, R.J., Poholek, A.C., DiToro, D., Yusuf, I., Eto, D., Barnett, B., Dent, A.L., Craft, J., and Crotty, S. (2009). Bcl6 and Blimp-1 are reciprocal and antagonistic regulators of T follicular helper cell differentiation. Science *325*, 1006–1010.

Johnston, R.J., Choi, Y.S., Diamond, J.A., Yang, J.A., and Crotty, S. (2012). STAT5 is a potent negative regulator of TFH cell differentiation. J. Exp. Med. *209*, 243–250.

Kim, C.H., Rott, L.S., Clark-Lewis, I., Campbell, D.J., Wu, L., and Butcher, E.C. (2001). Subspecialization of CXCR5+ T cells: B helper activity is focused in a germinal center-localized subset of CXCR5+ T cells. J. Exp. Med. *193*, 1373–1381.

Kroenke, M.A., Eto, D., Locci, M., Cho, M., Davidson, T., Haddad, E.K., and Crotty, S. (2012). Bcl6 and Maf cooperate to instruct human follicular helper CD4 T cell differentiation. J. Immunol. *188*, 3734–3744.

Kwon, H., Thierry-Mieg, D., Thierry-Mieg, J., Kim, H.P., Oh, J., Tunyaplin, C., Carotta, S., Donovan, C.E., Goldman, M.L., Tailor, P., et al. (2009). Analysis of interleukin-21-induced Prdm1 gene regulation reveals functional cooperation of STAT3 and IRF4 transcription factors. Immunity *31*, 941–952.

Linterman, M.A., Rigby, R.J., Wong, R., Silva, D., Withers, D., Anderson, G., Verma, N.K., Brink, R., Hutloff, A., Goodnow, C.C., and Vinuesa, C.G. (2009a). Roquin differentiates the specialized functions of duplicated T cell costimulatory receptor genes CD28 and ICOS. Immunity *30*, 228–241.

Linterman, M.A., Rigby, R.J., Wong, R.K., Yu, D., Brink, R., Cannons, J.L., Schwartzberg, P.L., Cook, M.C., Walters, G.D., and Vinuesa, C.G. (2009b). Follicular helper T cells are required for systemic autoimmunity. J. Exp. Med. *206*, 561–576.

Lüthje, K., Kallies, A., Shimohakamada, Y., Belz, G.T., Light, A., Tarlinton, D.M., and Nutt, S.L. (2012). The development and fate of follicular helper T cells defined by an IL-21 reporter mouse. Nat. Immunol. *13*, 491–498.

Mestas, J., Crampton, S.P., Hori, T., and Hughes, C.C. (2005). Endothelial cell co-stimulation through OX40 augments and prolongs T cell cytokine synthesis by stabilization of cytokine mRNA. Int. Immunol. *17*, 737–747.

Murata, K., Nose, M., Ndhlovu, L.C., Sato, T., Sugamura, K., and Ishii, N. (2002). Constitutive OX40/OX40 ligand interaction induces autoimmune-like diseases. J. Immunol. *169*, 4628–4636.

Murray, S.E., Polesso, F., Rowe, A.M., Basak, S., Koguchi, Y., Toren, K.G., Hoffmann, A., and Parker, D.C. (2011). NF-κB–inducing kinase plays an essential T cell–intrinsic role in graft-versus-host disease and lethal autoimmunity in mice. J. Clin. Invest. *121*, 4775–4786.

Nakayamada, S., Kanno, Y., Takahashi, H., Jankovic, D., Lu, K.T., Johnson, T.A., Sun, H.W., Vahedi, G., Hakim, O., Handon, R., et al. (2011). Early Th1 cell differentiation is marked by a Tfh cell-like transition. Immunity *35*, 919–931.

Nurieva, R.I., Chung, Y., Martinez, G.J., Yang, X.O., Tanaka, S., Matskevitch, T.D., Wang, Y.H., and Dong, C. (2009). Bcl6 mediates the development of T follicular helper cells. Science *325*, 1001–1005.

Nurieva, R.I., Podd, A., Chen, Y., Alekseev, A.M., Yu, M., Qi, X., Huang, H., Wen, R., Wang, J., Li, H.S., et al. (2012). STAT5 protein negatively regulates T follicular helper (Tfh) cell generation and function. J. Biol. Chem. *287*, 11234–11239.

Rolf, J., Bell, S.E., Kovesdi, D., Janas, M.L., Soond, D.R., Webb, L.M., Santinelli, S., Saunders, T., Hebeis, B., Killeen, N., et al. (2010). Phosphoinositide 3-kinase activity in T cells regulates the magnitude of the germinal center reaction. J. Immunol. *185*, 4042–4052.

Sasaki, Y., Calado, D.P., Derudder, E., Zhang, B., Shimizu, Y., Mackay, F., Nishikawa, S., Rajewsky, K., and Schmidt-Supprian, M. (2008). NIK overexpression amplifies, whereas ablation of its TRAF3-binding domain replaces BAFF:BAFF-R-mediated survival signals in B cells. Proc. Natl. Acad. Sci. USA *105*, 10883–10888.

Schneider, K., Potter, K.G., and Ware, C.F. (2004). Lymphotoxin and LIGHT signaling pathways and target genes. Immunol. Rev. *202*, 49–66.

Siess, D.C., Vedder, C.T., Merkens, L.S., Tanaka, T., Freed, A.C., McCoy, S.L., Heinrich, M.C., Deffebach, M.E., Bennett, R.M., and Hefeneider, S.H. (2000). A human gene coding for a membrane-associated nucleic acid-binding protein. J. Biol. Chem. *275*, 33655–33662.

Simpson, T.R., Quezada, S.A., and Allison, J.P. (2010). Regulation of CD4 T cell activation and effector function by inducible costimulator (ICOS). Curr. Opin. Immunol. *22*, 326–332.

So, T., Choi, H., and Croft, M. (2011). OX40 complexes with phosphoinositide 3-kinase and protein kinase B (PKB) to augment TCR-dependent PKB signaling. J. Immunol. *186*, 3547–3555.

Vinuesa, C.G., Cook, M.C., Angelucci, C., Athanasopoulos, V., Rui, L., Hill, K.M., Yu, D., Domaschenz, H., Whittle, B., Lambe, T., et al. (2005). A RING-type ubiquitin ligase family member required to repress follicular helper T cells and autoimmunity. Nature *435*, 452–458.

Wan, Y.Y., Leon, R.P., Marks, R., Cham, C.M., Schaack, J., Gajewski, T.F., and DeGregori, J. (2000). Transgenic expression of the coxsackie/adenovirus receptor enables adenoviral-mediated gene delivery in naive T cells. Proc. Natl. Acad. Sci. USA *97*, 13784–13789.

Weinberg, A.D. (2010). The role of OX40 (CD134) in T-cell memory generation. Adv. Exp. Med. Biol. *684*, 57–68.

Yu, D., Tan, A.H., Hu, X., Athanasopoulos, V., Simpson, N., Silva, D.G., Hutloff, A., Giles, K.M., Leedman, P.J., Lam, K.P., et al. (2007). Roquin represses autoimmunity by limiting inducible T-cell co-stimulator messenger RNA. Nature *450*, 299–303.

Yu, D., Rao, S., Tsai, L.M., Lee, S.K., He, Y., Sutcliffe, E.L., Srivastava, M., Linterman, M., Zheng, L., Simpson, N., et al. (2009). The transcriptional repressor Bcl-6 directs T follicular helper cell lineage commitment. Immunity *31*, 457–468.

Zheng, Y., Chaudhry, A., Kas, A., deRoos, P., Kim, J.M., Chu, T.T., Corcoran, L., Treuting, P., Klein, U., and Rudensky, A.Y. (2009). Regulatory T-cell suppressor program co-opts transcription factor IRF4 to control T(H)2 responses. Nature *458*, 351–356.